

---

# Crystallographic and biochemical studies revealing the structural basis for antizyme inhibitor function

---

SHIRA ALBECK,<sup>1,3</sup> ORLY DYM,<sup>1,3</sup> TAMAR UNGER,<sup>1,3</sup> ZOHAR SNAPIR,<sup>2</sup>  
ZIPPY BERCOVICH,<sup>2</sup> AND CHAIM KAHANA<sup>2</sup>

<sup>1</sup>The Israel Structural Proteomics Center, Weizmann Institute of Science, Rehovot 76100, Israel

<sup>2</sup>Department of Molecular Genetics, Weizmann Institute of Science, Rehovot 76100, Israel

(RECEIVED December 26, 2007; FINAL REVISION January 28, 2008; ACCEPTED January 29, 2008)

## Abstract

Antizyme inhibitor (AzI) regulates cellular polyamine homeostasis by binding to the polyamine-induced protein, Antizyme (Az), with greater affinity than ornithine decarboxylase (ODC). AzI is highly homologous to ODC but is not enzymatically active. In order to understand these specific characteristics of AzI and its differences from ODC, we determined the 3D structure of mouse AzI to 2.05 Å resolution. Both AzI and ODC crystallize as a dimer. However, fewer interactions at the dimer interface, a smaller buried surface area, and lack of symmetry of the interactions between residues from the two monomers in the AzI structure suggest that this dimeric structure is nonphysiological. In addition, the absence of residues and interactions required for pyridoxal 5'-phosphate (PLP) binding suggests that AzI does not bind PLP. Biochemical studies confirmed the lack of PLP binding and revealed that AzI exists as a monomer in solution while ODC is dimeric. Our findings that AzI exists as a monomer and is unable to bind PLP provide two independent explanations for its lack of enzymatic activity and suggest the basis for its enhanced affinity toward Az.

**Keywords:** structure/function studies; protein crystallization; protein structures–new; antizyme inhibitor; antizyme; ornithine decarboxylase

Polyamines are small organic polycations that are essential for cell proliferation and play an important role in regulating other fundamental cellular processes. Elevated polyamine levels are observed in rapidly growing cells including transformed cells; thus, polyamine metabolism has been suggested as a potential target for cancer therapy (Pegg 1988; Marton and Pegg 1995; Wallace and Fraser 2004). The range of intracellular polyamines is determined at the lower limit by their absolute requirement for cellular proliferation and at the upper limit by their cytotoxicity (Poulin et al. 1993; Tobias and Kahana 1995), indicating a need for strict regulation of their intracellular concentration. Multiple pathways such as synthesis, up-

take, degradation, and efflux regulate cellular polyamine levels. Ornithine decarboxylase (ODC) is the first and rate-limiting enzyme in the polyamine biosynthesis pathway (Pegg 2006). It is a pyridoxal 5'-phosphate (PLP)-dependent enzyme that provides the only route for converting ornithine to putrescine. ODC, which is characterized by a short intracellular half-life, is part of an autoregulatory circuit mediated by a polyamine-induced protein, termed Antizyme (Az). An increased intracellular polyamine concentration increases the synthesis of Az by stimulating ribosomal frameshifting (Rom and Kahana 1994; Matsufuji et al. 1995). Az, in turn, binds to transient ODC monomer subunits with high affinity, preventing their re-association into active homodimers and targeting them for rapid degradation by the 26S proteasome (Murakami et al. 1992). Az also regulates polyamine transport across the plasma membrane via an unknown mechanism (He et al. 1994; Mitchell et al. 1994; Suzuki et al. 1994; Sakata et al. 2000).

---

<sup>3</sup>These authors contributed equally to this work.

Reprint requests to: Chaim Kahana, Department of Molecular Genetics, Weizmann Institute of Science, Rehovot 76100, Israel; e-mail: chaim.kahana@weizmann.ac.il; fax: +972-8-9344199.

Article published online ahead of print. Article and publication date are at <http://www.proteinscience.org/cgi/doi/10.1110/ps.073427208>.

An additional protein, termed Antizyme inhibitor (AzI), was demonstrated to regulate cellular polyamines and cellular proliferation, mainly by negating Az functions (Keren-Paz et al. 2006; Kim et al. 2006). AzI is highly homologous to ODC but does not display ODC activity (Murakami et al. 1996). AzI has a higher affinity for Az than ODC and therefore is able to sequester Az, resulting in reduced ODC degradation and enhanced polyamine uptake (Keren-Paz et al. 2006). Consequently, overexpression of AzI increases cellular polyamine levels, leading to increased cellular proliferation and to cellular transformation (Keren-Paz et al. 2006; Kim et al. 2006), while down-regulation of AzI results in inhibition of cellular proliferation (Choi et al. 2005; Keren-Paz et al. 2006). Thus, AzI is differentially expressed in gastric tumors compared to matched healthy tissue (Jung et al. 2000). While AzI promotes cell proliferation by negating Az functions, it was suggested that AzI might also act in an Az-independent manner (Kim et al. 2006).

Similar to ODC, AzI is also a rapidly degraded protein (Kitani and Fujisawa 1989; Bercovich and Kahana 2004); however, in contrast to ODC, AzI degradation is ubiquitin dependent and does not require interaction with Az or the C-terminal segment (Bercovich and Kahana 2004), which, in the case of ODC, serves as a proteasome-recognition signal (Zhang et al. 2003). In fact, interaction with Az actually stabilizes AzI by interfering with its ubiquitination (Bercovich and Kahana 2004).

Here, we describe the first crystal structure of AzI to 2.05 Å resolution. Structural comparison of mouse AzI to ODC from various species revealed that the dimer interface of AzI is very different from that of ODC; AzI has fewer interactions in its dimer interface, a smaller buried surface area, and nonsymmetric interactions between residues from the two monomers. These findings support a nonphysiological dimer in the crystal, which was confirmed by biochemical studies, demonstrating that AzI exists as a monomer in solution. The crystal structure and biochemical experiments also show that AzI does not bind PLP. These findings provide the structural basis for the lack of ornithine decarboxylating activity of AzI and support its primary role in negating Az functions.

## Results and Discussion

### Overall structure of AzI

Mouse full-length AzI (residues 1–448) was produced in *Escherichia coli* and purified to homogeneity. AzI crystallized as a dimer in the asymmetric unit cell (observed electron density for residues 8–435 for each monomer) (Fig. 1A). Each monomer consists of two domains: a TIM-like  $\alpha/\beta$ -barrel domain (residues 45–280) and a modified Greek key  $\beta$ -sheet domain (residues 8–44 and

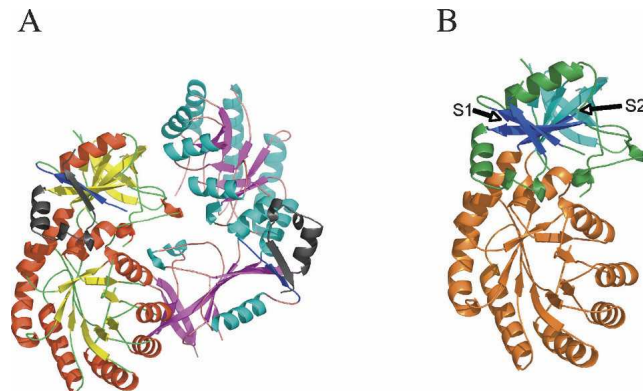


**Figure 1.** Crystal structure of AzI. (A) Ribbon representation of the AzI homodimer. Helices are colored in red and  $\beta$  strands in yellow in monomer A (left) and in cyan and magenta, respectively, in monomer B (right). The N termini are colored blue, and the C termini are gray. (B) Monomer of AzI showing its two domains: TIM  $\alpha/\beta$ -barrel domain (residues 45–280) (orange) and a modified Greek key  $\beta$ -sheet domain (residues 8–44 and 281–435, with its helices in green and two sheets—S1 and S2—in blue and cyan, respectively). The figure was created using PyMOL (DeLano Scientific).

281–435) (Fig. 1B). The TIM barrel domain is composed of eight parallel strands followed by  $\alpha$ -helices in the following order:  $\alpha_2\beta_3$ ,  $\eta_1\alpha_3\beta_4$ ,  $\alpha_4\eta_2\beta_5$ ,  $\alpha_5\beta_6$ ,  $\alpha_6\beta_7$ ,  $\alpha_7\beta_8$ ,  $\alpha_8\beta_9$ , and  $\alpha_9\beta_{10}$ . The sheet domain is composed of two sheets (S1 and S2) that are perpendicular to each other and five helices ( $\alpha_1$ ,  $\eta_3$ ,  $\alpha_{11}$ ,  $\eta_5$ , and  $\eta_6$ ). The S1 sheet is composed of four parallel strands,  $\beta_1\downarrow$ ,  $\beta_2\downarrow$ ,  $\beta_{17}\downarrow$ , and  $\beta_{18}\downarrow$ . S2 consists of six antiparallel strands,  $\beta_{11}\uparrow$ ,  $\beta_{12}\downarrow$ ,  $\beta_{13}\uparrow$ ,  $\beta_{14}\downarrow$ ,  $\beta_{15}\uparrow$ , and  $\beta_{16}\downarrow$ , and is connected to S1 by  $\eta_4$ . The two monomers are essentially identical, with RMSD of 0.35 Å for all C $\alpha$  atoms. The structure of AzI has several disordered regions. These include the first seven residues at the N terminus, the last 13 residues at the C terminus, and three disordered loops: amino acids 160–167, which connect  $\beta_7$  to  $\alpha_7$ ; 294–310, connecting  $\beta_{11}$  to  $\beta_{12}$ ; and 330–334 between  $\eta_3$  to  $\beta_{13}$ .

### Comparison of the AzI structure to that of ODCs

A primary sequence alignment and structural comparison of AzI to mouse (Kern et al. 1999), human (Almud et al. 2000), and trypanosome (Jackson et al. 2000) ODC (mODC, hODC, and tODC, respectively) reveal high sequence identity (~50%) and structural similarity between AzI and ODC monomers from these different species (RMSD values of 1.85 Å, 1.6 Å, and 1.5 Å, respectively) (Figs. 2, 3A). Significant conformational differences between AzI and the ODC structure lie in the two loops positioned at the dimer interface (AzI residues 355–362 and 387–401) (Fig. 3B) and in the N and C termini (AzI residues 8–17 and 409–435, respectively) (Fig. 3C). The N terminus of the AzI structure begins at residue 8



**Figure 2.** Sequence alignment of mAzI, mODC, hODC, and tODC (numbering refers to the sequence of AzI). AzI secondary-structure elements are labeled *above* the corresponding sequence;  $\alpha$ -helices are indicated by spirals, and  $\beta$  strands by arrows. Residues conserved in all four proteins appear in red blocks. The figure was created using ESPrnt (Gouet et al. 1999).

forming a  $\beta$  strand ( $\beta$ 1) that is well aligned with the corresponding  $\beta$  strand of all the ODC structures (Figs. 2, 3C). While no electron density is observed for the first few residues of the N terminus of the AzI, hODC, and tODC structures, in mODC, this region is structured, as residues 3–6 form a  $\beta$  strand ( $\beta$ -1) (Fig. 3C). Electron density is observed at the C terminus of AzI (between residues 428 and 435), which is absent in all the ODC structures. Interestingly, this extra segment forms a  $\beta$  strand ( $\beta$ 18), which is in close proximity to  $\beta$ 1 formed by the N terminus (Figs. 1A, 3C). This arrangement allows

stabilizing interactions between the AzI termini. In contrast to AzI, the ODC structures lack electron density in their C termini, yielding a large separation between the N and C termini. This in turn may facilitate the exposure of the seemingly unstructured ODC C terminus upon interaction with Az (Li and Coffino 1993).

#### *Structure of AzI suggests its existence as a monomer in solution*

AzI crystallizes as a dimer such that the two monomers adopt a head-to-tail orientation as observed in the ODC

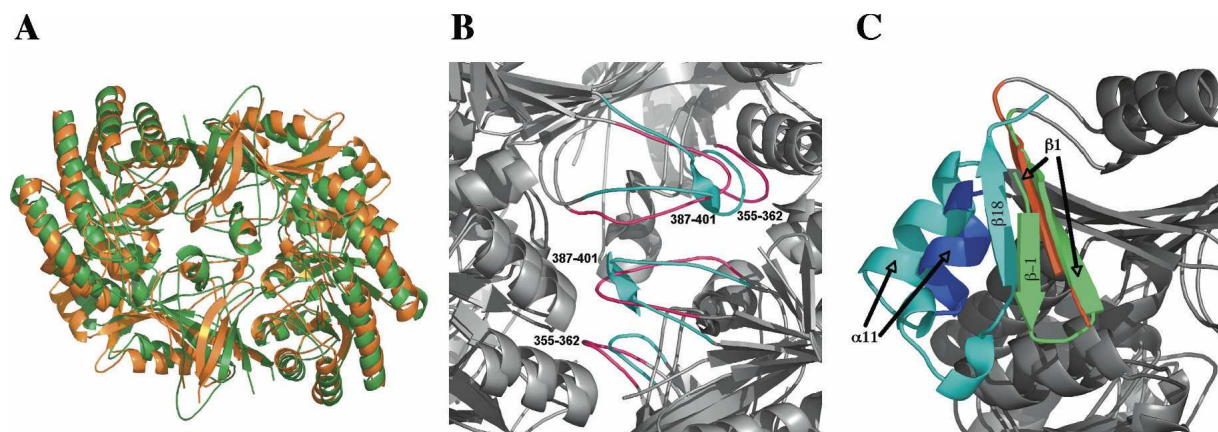


**Figure 3.** Comparison of AzI and mODC structures. (A) Superposition of the AzI crystallographic dimer (orange) and the mODC dimer (green) (PDB code 7ODC). (B) Superposition of the interface of mAzI and mODC showing the variable loops between monomers A and B and between monomers B and A (AzI residues 355–362 and 387–401). AzI loops are in cyan, and ODC loops are in magenta. (C) Comparison of the N and C termini in the structures of AzI and mODC. AzI N-terminal  $\beta 1$  is in red, and C-terminal  $\beta 18$  in cyan; mODC N-terminals  $\beta -1$  and  $\beta 1$  are in green and C-terminal  $\alpha 11$  in blue.  $\beta -1$  designates the additional  $\beta$  strand present in the N terminus of ODC, whereas  $\beta 18$  designates the extra  $\beta$  strand at the C terminus of AzI.

dimer. The two monomers of AzI exhibit only 43 contacts (up 3.5 Å), while significantly more contacts are observed between the two monomers of hODC, mODC, and tODC (83, 74, and 69, respectively). Furthermore, the surface area buried by the two AzI monomers is smaller than that buried by the mODC monomers (1492 Å<sup>2</sup> per monomer compared to 2284 Å<sup>2</sup>, which are 8% and 13% of the solvent accessible area, respectively, calculated by PISA [Krissinel and Henrick 2007]). These properties support a very loose crystallographic dimer.

A detailed analysis of all the interactions in the dimer interface of AzI and mODC demonstrates that the two dimer interfaces are characterized by different interactions, as shown in Table 1. It has been shown that the monomer association of tODC is driven by small energetic contributions of residues distributed throughout the ODC interface (Myers et al. 2001). Most of the interactions shown to contribute to ODC dimerization are not present in AzI. In fact, many of the interactions in AzI are unique, with the exception of that occurring between K141 and I288. Superposition of the two structures reveals significant conformational differences in two loops between residues 355–362 and 387–401 (Fig. 3B). Most of the unique interactions in AzI involve residues from these loops. Many of the interactions in the ODC interface involve residues that are conserved among the ODCs from various species but are different in AzI. Moreover, even those that are conserved in AzI do not participate in interdimer interactions (highlighted residues in Table 1). These include the two salt bridges, K169–D364 and D134–K294, which stabilize the ODC homodimer (Kern et al. 1999). In AzI, all four residues are conserved, yet these two salt bridges are not formed. A careful inspection of the AzI dimer interface demon-

strates that the two monomers are further apart compared to those of ODC, preventing the formation of these interactions.

Conserved hydrophobic residues in ODC form a zipper that stabilizes its homodimeric structure (Kern et al. 1999; Myers et al. 2001). These residues include F397(B), Y323(B), Y331(A), Y331(B), Y323(A), and F397(A) (A and B correspond to the two monomers, respectively) (Fig. 4A). Y331, an important residue in the ODC zipper, is changed to S329 in AzI and interferes with the formation of a similar zipper in AzI (Fig. 4B). The ODC dimer is further stabilized by multiple interactions formed by Y331 with V322, Y323, N327, and L330 of the opposite monomer. Thus, in AzI, where Y331 is a serine, neither these multiple interactions nor formation of the hydrophobic zipper can occur.

As opposed to the ODC dimer, the crystallographic dimer of AzI lacks symmetry between its interactions. In the ODC dimer, all the interactions between residues from monomer A with B are reflected in reciprocal interactions from B to A, creating a twofold symmetry that is often observed in physiological dimers (Table 1) (Goodsell and Olson 2000). The only three symmetrical interactions in AzI involve residue D397 (which forms multiple interactions with residues of the opposite monomer) and interactions K141–I288 and E391–A394 (Table 1). Consequently, the AzI dimer is not symmetrical, further suggesting that the dimeric structure is not maintained in solution.

Our findings of a small number of interdimer contacts, a small buried surface area, missing salt bridges, absence of hydrophobic zipper and the lack of symmetry between the interactions, all suggest that the dimeric structure of the AzI crystal is nonphysiological.

**Table 1.** Comparison of the interactions between residues from monomer A to monomer B in mAzI and mODC crystal structures (up to 3.5 Å) (Fig. 2)<sup>a</sup>

mAzI		mODC		Conservation	
A	B	A	B	ODC <sup>b</sup>	AzI <sup>c</sup>
		D36	Q116, S118	+	–
		D38	Q116	+	–
		<b>K69</b>	<b>C358(360), F395(397)</b>	+	+
			<b>N396(398)</b>		
		A90	N396(398)	+	–
		<b>S91 E94</b>	<b>N396(398)</b>	+	+
S91, K92, N93	D397			–	–
Q119					
		T93	G397(399) Q399(401)	+	–
Q116	I288	Q116	N317(319), D38, D36	+	–
		S118	D36	+	–
		<b>D134</b>	<b>K291(294)</b>	+	+
K141	I288	K141	I288(291)	+	+
		<b>K169</b>	<b>K291(294), Y315(317)</b>	+	+
			<b>G355(357), D359(361)</b>		
			<b>D362(364)</b>		
			T357(359)	+	–
F170	C358			+	+
I288	K141	I288(291)	K141	+	+
		<b>K291(294)</b>	<b>D134, K169</b>	+	+
		<b>Y315(317)</b>	<b>K169</b>	+	+
		<b>N317(319)</b>	<b>Q116</b>	+	+
		V320(322)	Y329(331)	+	–
		Y321(323)	Y329(331)	+	–
		N325(327)			
		L328(330)			
S329	E360	Y329(331)	V320(322), Y321(323), L328(330), N325(327)	+	–
		<b>G355(357)</b>	<b>K169</b>	+	+
		T357(359)	K169	+	–
C358	C114			+	+
	M168			–	+
		<b>C358(360)</b>	<b>K69</b>	+	+
		<b>D359(361)</b>	<b>K169</b>	+	+
E360	M168	<b>D362(364)</b>	<b>K169</b>	+	–
H390	F395			+	–
E391	S393, A394			–	–
A394	E391			–	–
		<b>F395(397)</b>	<b>K69</b>	+	+
		N396(398)	A90	+	–
		<b>N396(398)</b>	<b>S91, K69, E94</b>	+	+
D397	S91, N93, K92			–	–
	Q119				
		G397(399)	T93	+	–
F398	E391			+	–
	N93			+	–
Q399	K92	Q399(401)	T93	+	–

<sup>a</sup>All numbering corresponds to the sequence of AzI. Numbering in parentheses corresponds to mODC.

<sup>b</sup>ODC corresponds to the conservation of the interacting residues among ODCs from mouse, human, and trypanosoma.

<sup>c</sup>AzI corresponds to the conservation of the interacting residues in AzI compared to ODC.

*Biochemical studies demonstrate that AzI exists as a monomer in solution*

In its active form, ODC is a homodimer that contains two active sites located at the interface between its subunits

(Tobias and Kahana 1993; Coleman et al. 1994). In solution, ODC exists in equilibrium between active dimers and inactive monomers (Pegg 2006). As AzI has no ornithine decarboxylating activity we set out to determine whether AzI exists in solution as a dimer or a

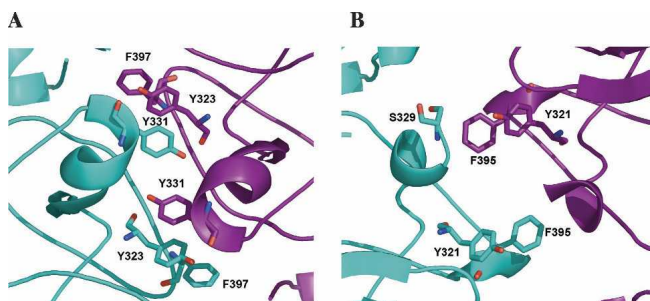


**Figure 4.** Comparison of homodimer interfaces of mODC (PDB code 7ODC) and AzI structures showing side chains that form contacts (up to 3.5 Å) (monomer A in cyan, and monomer B in purple). The figure was created using PyMOL (DeLano Scientific). (A) mODC residues that form the hydrophobic zipper. (B) mAzI showing the absence of the hydrophobic zipper.

monomer. Cross-linking analysis failed to demonstrate AzI dimers while readily revealing ODC dimers (Fig. 5A), suggesting that AzI exists predominantly in a monomeric state. This was further confirmed by comparing the migration of recombinant AzI and ODC proteins on a size-exclusion column; our results showed that, while ODC migrated predominantly as a dimer with a small proportion of monomers, AzI migrated solely as a monomer (Fig. 5B). These results demonstrate that under physiological conditions, AzI is a monomer. This supports our structural study indicating that AzI is a non-physiological dimer. This phenomenon of proteins that crystallize as nonspecific dimers while physiologically existing as a monomer is well documented in the literature (Bahadur et al. 2004; Dafforn 2007).

AzI is a regulator of Az, which in turn regulates ODC. This delicate regulatory process is fine-tuned by the different affinity that these two proteins have toward Az. As opposed to ODC monomers that are known to bind Az, ODC dimers do not interact with Az (Mitchell and Chen 1990). Active ODC dimers have been shown to be in rapid equilibrium with inactive monomers, providing a pool of monomers, which are needed for ODC regulation by Az. We, therefore, suggest that the fact that AzI is always a monomer, makes it more available for this interaction, and contributes to the higher affinity of AzI toward Az.

#### *AzI does not bind PLP*

PLP-dependent enzymes have conserved active-site residues and secondary-structural features, implying that they have similar PLP binding sites (Momany et al. 1995). A comparative analysis of the structures of AzI versus those of ODC suggests that AzI does not bind PLP. Many of the residues involved in mediating PLP binding in ODC are not conserved in AzI. These include D88A, R154H, R277S, D332E, and Y389D (ODC residue numbering followed by the amino acid in AzI) (Kern et al.

1999). Thus, the environment formed by AzI is different than that of ODC, possibly preventing important interactions between AzI and PLP (Fig. 6). It is important to note in this respect that the loss of even one of these interactions, as exemplified in the ODC R277A mutant, results in a 100-fold decrease in PLP binding as well as a 50% drop in  $K_{cat}$  and a sevenfold decrease in  $K_M$  (Osterman et al. 1997).

Therefore, we tested the structural prediction that AzI may lack ODC activity due to inability to bind PLP. Two independent experimental approaches were used to determine whether AzI binds PLP. In the first, both ODC and AzI were translated in vitro in reticulocyte lysate and were tested for their ability to bind to pyridoxamine phosphate (PMP) beads, and the ability of PLP to displace this interaction (Boucek Jr. and Lembach 1977). In contrast to ODC, which efficiently bound to the PMP

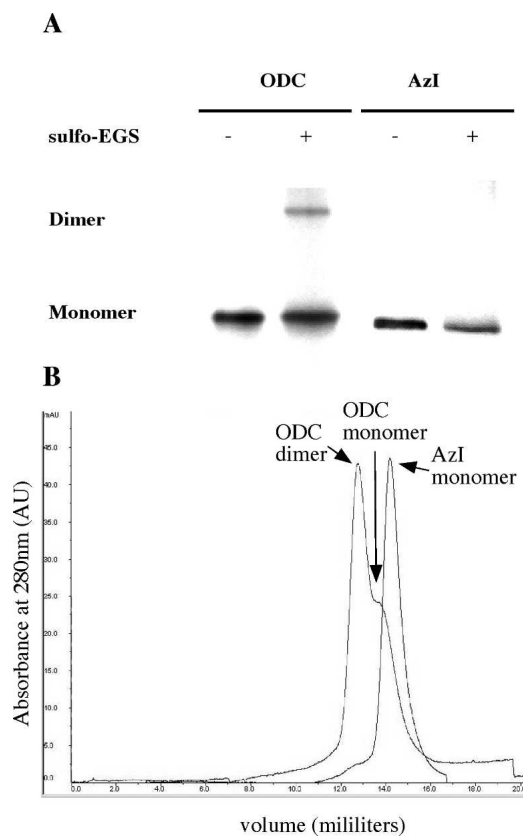


**Figure 5.** AzI exists as a monomer in solution. (A) SDS-PAGE of AzI and ODC following cross-linking. (B) Size-exclusion chromatogram of mAzI compared to mODC. Each protein (50 µg) was injected into a Superdex 200 HR 10/30 column (GE Healthcare) in a buffer containing 50 mM Tris pH 7.5, 0.1 M NaCl, and 1 mM DTT. The elution positions of monomers and dimers of ODC and AzI are indicated by arrows (molecular weight standards [Amersham Biosciences] migrated under the same conditions, as follows: aldolase [ $M_r$  158,000] at 12.5 mL, albumin [ $M_r$  67,000] at 13.7 mL, and ovalbumin [ $M_r$  43,000] at 14.8 mL).

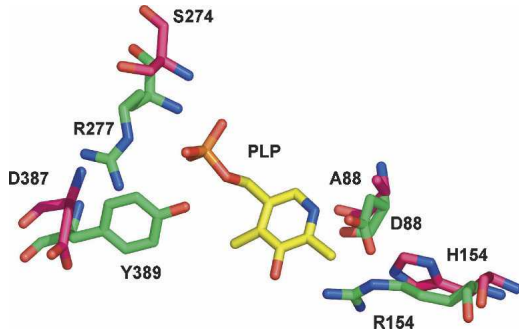


**Figure 6.** Comparison of PLP-binding site in ODC to the corresponding residues in Azi. Residues are depicted by sticks; PLP is in yellow, ODC residues D88, R154, R277, and Y389 are in green, and corresponding Azi residues A88, H154, S274, and D387 are in magenta. The figure was created using PyMOL (DeLano Scientific).

beads, and was eluted by PLP, no Azi binding was noted (Fig. 7A). The second method is based on direct determination of bound PLP in proteins (Adams 1979). Equal amounts of ODC and Azi were incubated in a buffer containing PLP, and unbound PLP was then removed by dialysis. Fluorometric measurement of PLP released from the protein after trichloroacetic acid precipitation revealed that, while an equimolar amount of PLP was released from ODC, no PLP was released from Azi (Fig. 7B). Thus, we conclude that Azi does not bind PLP.

### Conclusion

In this study we identified two independent properties underlying the lack of ornithine decarboxylating activity by Azi. While its sequence and structure are highly homologous to those of ODC, Azi does not bind PLP, and it does not form dimers. Both properties have been demonstrated here biochemically and rationalized structurally. The fact that Azi exists only as a monomer excludes the possibility of it functioning as an enzyme but does provide it with an advantage toward its primary function, namely, regulating Az. ODC on the other hand, is in equilibrium between active dimers and inactive monomers that are available for Az binding. This delicate regulatory process is tuned by the enhanced affinity of Azi toward Az, compared to that of ODC. Once bound, Az stabilizes Azi by interfering with its ubiquitination. Solving the structure of the Az–Azi complex may shed light on the mechanism of this stabilization process.

### Materials and Methods

#### Expression and purification of selenomethionine recombinant Azi

Full-length Azi was cloned into pETG-20A (a gift from A. Gerloff, EMBL Hamburg, Germany) by recombination using

the Gateway system. Azi was produced as an N-terminal Trx-6His fusion that included a tobacco etch virus (TEV) protease cleavage site to allow removal of the Trx-6His tag. BL21(DE3) bacteria expressing pETG20-Trx-His-TEV-Azi were grown at 37°C in M9 minimal medium containing glucose (0.4 w/v) and ampicillin (100 mg/mL). When cultures reached  $A_{600} = 0.6$ , the following substances were added as solids per 1 L of culture; selenomethionine (50 mg), along with lysine hydrochloride (100 mg), threonine (100 mg), phenylalanine (100 mg), leucine (50 mg), isoleucine (50 mg), and valine (50 mg). Protein expression was induced with 100  $\mu$ M of isopropyl-1-thio- $\beta$ -D-galactopyranoside (IPTG) at 15°C for 24 h. Bacteria were lysed by sonication in 50 mM Tris-HCl pH 7.5, 500 mM NaCl, and 1 mM PMSF, protease inhibitor cocktail (Calbiochem) in the presence of DNase (1  $\mu$ g/mL) and lysosyme (40 U/mL culture). Soluble protein was purified using a Ni-NTA column (HiTrap chelating HP, Amersham) followed by gel filtration chromatography (HiLoad 16/60 Superdex 200, Amersham) in 50 mM Tris pH 7.5, 0.1 M NaCl, and 1 mM DTT. Pooled fractions containing Azi were then purified by ion-exchange chromatography (Tricorn Q 10/100GL, Amersham). The recombinant protein was cleaved by TEV protease overnight at 4°C, followed by an additional Ni-NTA column purification to remove excess TEV, the Trx-His fusion, and the uncleaved protein. The cleaved purified protein was passed through a HiPrep 26/10 desalting column in 20 mM Tris 7.5, 50 mM NaCl, and 5 mM DTT and concentrated to 13 mg/mL for crystallization experiments.

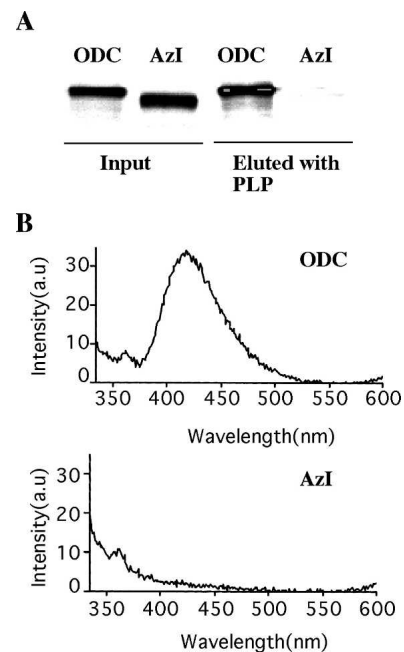


**Figure 7.** Azi does not bind PLP. (A) Equal amounts of in vitro-translated ODC and Azi were bound to PMP beds and eluted with PLP as described in Materials and Methods. The eluted material was fractionated by SDS-polyacrylamide gel electrophoresis, and the radioactive bands were visualized using a Fuji BAS 2500 phosphorimager. (B) Pyridoxal phosphate was released from recombinant ODC and Azi, and determined fluorometrically as described in Materials and Methods.

## Crystallization, data collection, and refinement

Crystals of AzI were obtained by the microbatch method (Chayen et al. 1992), under oil, using the Oryx6 robot (Douglas Instruments Ltd.). Selenomethionine AzI crystals were grown from a precipitating solution of 100 mM Tris pH 8, 16% PEG 6000 and 0.2 M CaCl<sub>2</sub>, and 14 mM 6-dimethyl-4-heptyl-β-D-maltoside. Crystals formed in space group *P*2<sub>1</sub>2<sub>1</sub>2, with cell constants *a* = 92.98 Å, *b* = 98.46 Å, and *c* = 117.49 Å, and contained two monomers in the asymmetric unit cell with *V*<sub>m</sub> of 2.71 Å<sup>3</sup>/Da. Multiple-wavelength anomalous diffraction data from a single crystal were collected at the European Synchrotron Radiation Facility (ESRF) beamline, ID 14-4. Bijvoet pairs to 2.04 Å resolution were collected at the peak, inflection, and at a remote wavelength. The diffraction images were indexed and integrated using the program HKL2000 (Otwinowski and Minor 1997). The integrated reflections were scaled using the program SCALEPACK (Otwinowski and Minor 1997). Structure factor amplitudes were calculated using TRUNCATE from the CCP4 program suite (French and Wilson 1978). Details of the data collection are described in Table 2. Selenium sites were identified with the programs SOLVE (Terwilliger and Berendzen 1997) and RESOLVE (Terwilliger 2000, 2003) as implemented in the program PHENIX. All steps of atomic refinement were carried out with the program CCP4/Refmac5 (Murshudov et al. 1997). Calculations of overall anisotropic temperature factors and noncrystallographic symmetry restraints were performed throughout all the refinement steps. The model was built to  $2F_{\text{obs}} - F_{\text{calc}}$ , and  $F_{\text{obs}} - F_{\text{calc}}$  maps using the program COOT (Emsley and Cowtan 2004). In later rounds of refinement, water

molecules were built into peaks greater than  $3\sigma$  in  $F_{\text{obs}} - F_{\text{calc}}$  maps. The current model includes residues 8–159, 168–293, 311–329, 334–341, 348–435, and 193 water molecules. The electron density map of AzI shows a strong symmetric peak, of  $\sim 7\sigma$ , situated at the crystallographic axis. This density could not be accounted for, as none of the molecules present in the crystallization condition exhibit a symmetric structure. The  $R_{\text{free}}$  value is 24.07% (for the 5% of reflections not used in the refinement), and the  $R_{\text{work}}$  value is 19.97% for all data to 2.05 Å. The AzI model was evaluated with the program PROCHECK (Laskowski et al. 1993). Details of the refinement statistics of the AzI structure are described in Table 2. The coordinates and structure factors for AzI have been deposited in the RCSB Protein Data Bank under accession number 3BTN. All figures depicting structures were prepared using PyMOL (DeLano Scientific). Sequence alignment was performed using ESPript (Gouet et al. 1999).

## Determination of binding to pyridoxamine-5'-phosphate

Pyridoxamine 5'-phosphate (PMP) was coupled to AffiGel 10 (Bio-Rad) according to the manufacturer's instructions. In brief, 1 g of matrix was washed with 100 mL of cold, deionized water. The washed matrix was incubated with 200 mg of PMP in 0.1 M sodium phosphate buffer, pH 7.0, for 24 h at 4°C with continuous agitation. Unreacted groups were blocked by incubation with 1 M ethanolamine (pH 8.0) for 1 h; the gel was washed with 1 M NaCl in 10 mM sodium phosphate buffer, pH 7.0, and stored in 10 mM sodium phosphate buffer. <sup>35</sup>S-labeled proteins were incubated with

Table 2. Crystallographic data and refinement statistics

	Se peak	Se inflection	Se remote
Data collection			
Wavelength (Å)	0.979	0.98	0.976
Resolution (last shell), Å	50–2.04 (2.11)	50–2.15 (2.23)	50–2.30 (2.38)
Total no. of reflections	1,540,586	800,603	835,146
No. of unique reflections	68,784 (6769)	59,332 (5834)	48,789 (4791)
Completeness (last shell), %	100 (99.8)	100 (100)	100 (100)
$R_{\text{sym}}$ , % <sup>a</sup>	9.4 (41.8)	7.3 (41.1)	7.1 (36.6)
$R_{\text{mrg}}$ , % <sup>b</sup>	7.5 (39.8)	5.8 (37.6)	5.8 (34.4)
Avg. $I/\sigma$	6 (5.8)	5 (4.5)	5 (5.1)
Refinement statistics			
$I/\sigma$ cutoff	0		
$R_{\text{work}}$ <sup>c</sup>	19.7%		
$R_{\text{free}}$ <sup>d</sup>	24.07%		
Mean <i>B</i> value (Å <sup>2</sup> )	28.46		
Total no. of atoms	6283		
RMSD bond (Å)	0.035		
RMSD angle (°)	2.53		
Ramachandran statistics			
Most favored (%)	91.8		
Additional allowed (%)	8.1		
Generously allowed (%)	0.1		

<sup>a</sup>  $R_{\text{sym}} = \frac{\sum \langle I_{hkl} \rangle - I_{hkl}}{\sum I_{hkl}}$ , where  $\langle I_{hkl} \rangle$  is the average intensity over symmetry-related reflections and  $I_{hkl}$  is the observed intensity.

<sup>b</sup>  $R_{\text{mrg}} = \frac{\sum (I_{hkl} - \langle I_{hkl} \rangle)^2 / \langle I_{hkl} \rangle^2}{\sum I_{hkl}}$ , where  $\langle I_{hkl} \rangle$  is the average intensity over symmetry-related reflections and  $I_{hkl}$  is the observed intensity.

<sup>c</sup>  $R_{\text{work}} = \frac{\sum ||F_o| - |F_c||}{\sum |F_o|}$ , where  $F_o$  denotes the observed structure factor amplitude and  $F_c$  the structure factor calculated from the model.

<sup>d</sup>  $R_{\text{free}}$  is for 5% of randomly chosen reflections excluded from the refinement.

150  $\mu$ L of PMP agarose beads in incubation buffer (25 mM Tris-HCl pH 7.5, 10 mM EDTA, 5 mM DTT) for 12 h at 4°C. The beads were washed three times with 1.5 mL of incubation buffer containing 15 mM KCl, and the bound material eluted with 40  $\mu$ L of incubation buffer containing 100 mM pyridoxal 5-phosphate by incubation for 60 min at 37°C.

#### Fluorimetric determination of pyridoxal phosphate

PLP bound to ODC and AzI was determined as described previously (Adams 1979). First, 50  $\mu$ g of AzI and ODC were incubated in ODC activity buffer (25 mM Tris-HCl pH 7.5, 2.5 mM DTT, 0.1 mM EDTA, containing 100 mM PLP), and unbound PLP was removed by dialysis. The proteins were diluted in 0.2 mL of 5 mM potassium phosphate buffer, pH 7.4. The samples were incubated for 15 min at 50°C following the addition of 0.2 mL of 11% trichloroacetic acid. Next, 140  $\mu$ L of 3.3 M  $K_2HPO_4$  and 50  $\mu$ L of 20 mM KCN were added, and the samples incubated for an additional 25 min at 50°C. Finally, 70  $\mu$ L of 28%  $H_3PO_4$  and 1 mL of 2 M KAc were added, and fluorescence was measured at an excitation wavelength of 325 nm and emission wavelength of 420 nm.

#### Cross-linking analysis

In vitro-translated [ $^{35}$ S]methionine-labeled ODC, AzI, and their derived mutants were incubated for 3 h at 25°C in 10 mM Tris-HCl, pH 7.1, either alone or with 1 mM ethylene glycol bis(sulfosuccinimidylsuccinate) (sulfo-EGS, Pierce). The cross-linking reaction was terminated by the addition of 0.1 volume of 0.5 M Tris-HCl, pH 7.5. The cross-linked material was mixed with protein gel sample buffer, heated to 100°C for 5 min, and fractionated by SDS-polyacrylamide gel electrophoresis. The labeled proteins were visualized using a Fuji BAS 2500 phosphorimager.

#### Acknowledgment

We thank Anna Branzburg and Yossi Jacobovitch from the Israel Structural Proteomics Center (ISPC) for their skilled assistance. We are grateful to Dr. Gordon Leonard, at the European Synchrotron Radiation Facility (ESRF), beamline ID14-4, whose outstanding efforts have made these experiments possible. We thank Professor Joel L. Sussman for helpful discussions and Professor Israel Silman for his critical reading of the manuscript. This work was supported by grants from the Israel Academy of Sciences and Humanities, and from the Y. Leon Benozio Institute for Molecular Medicine, the M.D. Moross Institute for Cancer Research, and the Leo and Julia Forchheimer Center for Molecular Genetics at the Weizmann Institute. C.K. is the incumbent of the Jules J. Mallon Professorial chair in Biochemistry. The structure was determined in collaboration with the Israel Structural Proteomics Center (ISPC), supported by The Israel Ministry of Science, Culture and Sport, the Divadol Foundation, the Neuman Foundation, and the European Commission Sixth Framework Research and Technological Development Programme (SPINE2-COMPLEXES Project, under contract no. 031220).

#### References

Adams, E. 1979. Fluorometric determination of pyridoxal phosphate in enzymes. *Methods Enzymol.* **62**: 407–410.

- Almud, J.J., Oliveira, M.A., Kern, A.D., Grishin, N.V., Phillips, M.A., and Hackert, M.L. 2000. Crystal structure of human ornithine decarboxylase at 2.1 Å resolution: Structural insights to antizyme binding. *J. Mol. Biol.* **295**: 7–16.
- Bahadur, R.P., Chakrabarti, P., Rodier, F., and Janin, J. 2004. A dissection of specific and non-specific protein-protein interfaces. *J. Mol. Biol.* **336**: 943–955.
- Bercovich, Z. and Kahana, C. 2004. Degradation of antizyme inhibitor, an ornithine decarboxylase homologous protein, is ubiquitin-dependent and is inhibited by antizyme. *J. Biol. Chem.* **279**: 54097–54102.
- Boucek Jr., R.J. and Lembach, K.J. 1977. Purification by affinity chromatography and preliminary characterization of ornithine decarboxylase from simian virus 40-transformed 3T3 mouse fibroblasts. *Arch. Biochem. Biophys.* **184**: 408–415.
- Chayen, N.E., Shaw Stewart, P.D., and Blow, D.M. 1992. Microbatch crystallization under oil—a new technique allowing many small-volume crystallization trials. *Cryst. Growth* **122**: 176–180.
- Choi, K.S., Suh, Y.H., Kim, W.H., Lee, T.H., and Jung, M.H. 2005. Stable siRNA-mediated silencing of antizyme inhibitor: Regulation of ornithine decarboxylase activity. *Biochem. Biophys. Res. Commun.* **328**: 206–212.
- Coleman, C.S., Stanley, B.A., Viswanath, R., and Pegg, A.E. 1994. Rapid exchange of subunits of mammalian ornithine decarboxylase. *J. Biol. Chem.* **269**: 3155–3158.
- Dafforn, T.R. 2007. So how do you know you have a macromolecular complex? *Acta Crystallogr. D Biol. Crystallogr.* **63**: 17–25.
- Emsley, P. and Cowtan, K. 2004. COOT: Model-building tools for molecular graphics. *Acta Crystallogr. D Biol. Crystallogr.* **60**: 2126–2132.
- French, G.S. and Wilson, K.S. 1978. On the treatment of negative intensity observations. *Acta Crystallogr. A* **34**: 517–525.
- Goodsell, D.S. and Olson, A.J. 2000. Structural symmetry and protein function. *Annu. Rev. Biophys. Biomol. Struct.* **29**: 105–153.
- Gouet, P., Courcelle, E., Stuart, D.I., and Metz, F. 1999. ESPript: Analysis of multiple sequence alignments in PostScript. *Bioinformatics* **15**: 305–308.
- He, Y., Suzuki, T., Kashiwagi, K., and Igarashi, K. 1994. Antizyme delays the restoration by spermine of growth of polyamine-deficient cells through its negative regulation of polyamine transport. *Biochem. Biophys. Res. Commun.* **203**: 608–614.
- Jackson, L.K., Brooks, H.B., Osterman, A.L., Goldsmith, E.J., and Phillips, M.A. 2000. Altering the reaction specificity of eukaryotic ornithine decarboxylase. *Biochemistry* **39**: 11247–11257.
- Jung, M.H., Kim, S.C., Jeon, G.A., Kim, S.H., Kim, Y., Choi, K.S., Park, S.I., Joe, M.K., and Kimm, K. 2000. Identification of differentially expressed genes in normal and tumor human gastric tissue. *Genomics* **69**: 281–286.
- Keren-Paz, A., Bercovich, Z., Porat, Z., Erez, O., Brener, O., and Kahana, C. 2006. Overexpression of antizyme-inhibitor in NIH3T3 fibroblasts provides growth advantage through neutralization of antizyme functions. *Oncogene* **25**: 5163–5172.
- Kern, A.D., Oliveira, M.A., Coffino, P., and Hackert, M.L. 1999. Structure of mammalian ornithine decarboxylase at 1.6 Å resolution: Stereochemical implications of PLP-dependent amino acid decarboxylases. *Structure* **7**: 567–581.
- Kim, S.W., Mangold, U., Waghorne, C., Mobascher, A., Shantz, L., Banyard, J., and Zetter, B.R. 2006. Regulation of cell proliferation by the antizyme inhibitor: Evidence for an antizyme-independent mechanism. *J. Cell Sci.* **119**: 2583–2591.
- Kitani, T. and Fujisawa, H. 1989. Purification and characterization of antizyme inhibitor of ornithine decarboxylase from rat liver. *Biochim. Biophys. Acta* **991**: 44–49.
- Krissinel, E. and Henrick, K. 2007. Inference of macromolecular assemblies from crystalline state. *J. Mol. Biol.* **372**: 774–797.
- Laskowski, R.A., MacArthur, M.W., Moss, D.S., and Thornton, J.M. 1993. PROCHECK: A program to check the stereochemical quality of protein structures. *J. Appl. Crystallogr.* **26**: 283–291.
- Li, X. and Coffino, P. 1993. Degradation of ornithine decarboxylase: Exposure of the C-terminal target by a polyamine-inducible inhibitory protein. *Mol. Cell Biol.* **13**: 2377–2383.
- Marton, L.J. and Pegg, A.E. 1995. Polyamines as targets for therapeutic intervention. *Annu. Rev. Pharmacol. Toxicol.* **35**: 55–91.
- Matsufuji, S., Matsufuji, T., Miyazaki, Y., Murakami, Y., Atkins, J.F., Gesteland, R.F., and Hayashi, S. 1995. Autoregulatory frameshifting in decoding mammalian ornithine decarboxylase antizyme. *Cell* **80**: 51–60.
- Mitchell, J.L. and Chen, H.J. 1990. Conformational changes in ornithine decarboxylase enable recognition by antizyme. *Biochim. Biophys. Acta* **1037**: 115–121.

- Mitchell, J.L., Judd, G.G., Bareyal-Leyser, A., and Ling, S.Y. 1994. Feedback repression of polyamine transport is mediated by antizyme in mammalian tissue-culture cells. *Biochem. J.* **299**: 19–22.
- Momany, C., Ghosh, R., and Hackert, M.L. 1995. Structural motifs for pyridoxal-5'-phosphate binding in decarboxylases: An analysis based on the crystal structure of the *Lactobacillus* 30a ornithine decarboxylase. *Protein Sci.* **4**: 849–854.
- Murakami, Y., Matsufuji, S., Kameji, T., Hayashi, S., Igarashi, K., Tamura, T., Tanaka, K., and Ichihara, A. 1992. Ornithine decarboxylase is degraded by the 26S proteasome without ubiquitination. *Nature* **360**: 597–599.
- Murakami, Y., Ichiba, T., Matsufuji, S., and Hayashi, S. 1996. Cloning of antizyme inhibitor, a highly homologous protein to ornithine decarboxylase. *J. Biol. Chem.* **271**: 3340–3342.
- Murshudov, G.N., Vagin, A.A., and Dodson, E.J. 1997. Refinement of macromolecular structures by the maximum-likelihood method. *Acta Crystallogr. D Biol. Crystallogr.* **53**: 240–255.
- Myers, D.P., Jackson, L.K., Ipe, V.G., Murphy, G.E., and Phillips, M.A. 2001. Long-range interactions in the dimer interface of ornithine decarboxylase are important for enzyme function. *Biochemistry* **40**: 13230–13236.
- Osterman, A.L., Brooks, H.B., Rizo, J., and Phillips, M.A. 1997. Role of Arg-277 in the binding of pyridoxal 5'-phosphate to *Trypanosoma brucei* ornithine decarboxylase. *Biochemistry* **36**: 4558–4567.
- Otwinowski, Z. and Minor, W. 1997. Processing of X-ray diffraction data collected in oscillation mode. *Methods Enzymol.* **276**: 307–326.
- Pegg, A.E. 1988. Polyamine metabolism and its importance in neoplastic growth and a target for chemotherapy. *Cancer Res.* **48**: 759–774.
- Pegg, A.E. 2006. Regulation of ornithine decarboxylase. *J. Biol. Chem.* **281**: 14529–14532.
- Poulin, R., Coward, J.K., Lakanen, J.R., and Pegg, A.E. 1993. Enhancement of the spermidine uptake system and lethal effects of spermidine over-accumulation in ornithine decarboxylase-overproducing L1210 cells under hypoosmotic stress. *J. Biol. Chem.* **268**: 4690–4698.
- Rom, E. and Kahana, C. 1994. Polyamines regulate the expression of ornithine decarboxylase antizyme in vitro by inducing ribosomal frame-shifting. *Proc. Natl. Acad. Sci.* **91**: 3959–3963.
- Sakata, K., Kashiwagi, K., and Igarashi, K. 2000. Properties of a polyamine transporter regulated by antizyme. *Biochem. J.* **347**: 297–303.
- Suzuki, T., He, Y., Kashiwagi, K., Murakami, Y., Hayashi, S., and Igarashi, K. 1994. Antizyme protects against abnormal accumulation and toxicity of polyamines in ornithine decarboxylase-overproducing cells. *Proc. Natl. Acad. Sci.* **91**: 8930–8934.
- Terwilliger, T.C. 2000. Maximum-likelihood density modification. *Acta Crystallogr. D Biol. Crystallogr.* **56**: 965–972.
- Terwilliger, T.C. 2003. Automated main-chain model building by template matching and iterative fragment extension. *Acta Crystallogr. D Biol. Crystallogr.* **59**: 38–44.
- Terwilliger, T.C. and Berendzen, J. 1997. Bayesian correlated MAD phasing. *Acta Crystallogr. D Biol. Crystallogr.* **53**: 571–579.
- Tobias, K.E. and Kahana, C. 1993. Intersubunit location of the active site of mammalian ornithine decarboxylase as determined by hybridization of site-directed mutants. *Biochemistry* **32**: 5842–5847.
- Tobias, K.E. and Kahana, C. 1995. Exposure to ornithine results in excessive accumulation of putrescine and apoptotic cell death in ornithine decarboxylase overproducing mouse myeloma cells. *Cell Growth Differ.* **6**: 1279–1285.
- Wallace, H.M. and Fraser, A.V. 2004. Inhibitors of polyamine metabolism: Review article. *Amino Acids* **26**: 353–365.
- Zhang, M., Pickart, C.M., and Coffino, P. 2003. Determinants of proteasome recognition of ornithine decarboxylase, a ubiquitin-independent substrate. *EMBO J.* **22**: 1488–1496.